



Increasing aspect ratio of particles suppresses buckling in shells formed by drying suspensions

Journal:	<i>Soft Matter</i>
Manuscript ID	SM-COM-08-2020-001467.R1
Article Type:	Communication
Date Submitted by the Author:	08-Sep-2020
Complete List of Authors:	Al Harraq, Ahmed; Louisiana State University, Cain Department of Chemical Engineering Bharti, Bhuvnesh; Louisiana State University, Cain Department of Chemical Engineering

COMMUNICATION

Increasing aspect ratio of particles suppresses buckling in shells formed by drying suspensions

Ahmed Al Harraq^a and Bhuvnesh Bharti^{*a}

Received 00th January 20xx,

Accepted 00th January 20xx

DOI: 10.1039/x0xx00000x

Solvent evaporation in unpinned droplets of colloidal suspensions leads to the formation of porous shells which buckle under the pressure differential imposed by drying. We investigate the role of aspect ratio of rod-shaped particles in suppressing such buckling instabilities. Longer, thinner rods pack into permeable shells with consequently lower Darcy's pressure and thus avoid buckling.

Drying colloidal suspensions on surfaces gives rise to a fascinating variety of patterns and structures ranging from the 'coffee-ring'¹ to complex fractals^{2–4}. Small changes in parameters such as the rate of evaporation, the wettability of the surface and the volume fraction of solids in the dispersion have dramatic effects on both drying behaviour and final structure^{5,6}. For example, altering the contact angle between droplet and substrate can impart mobility to the contact line going between the two extremes of pinned and unpinned evaporation modes⁷. The latter drying regime is an appealing template for self-assembly due to its simplicity and versatility in fabricating three-dimensional mesostructures of different size, shape and composition^{8,9}. Amongst its limitations is the onset of buckling of the dried self-assembled structure¹⁰: such mechanical instability represents for unpinned droplets an equivalent obstacle as the coffee-ring effect presents for patterning in pinned suspensions. The drying of a spherical, unpinned droplet containing particles analogously involves hydrodynamic effects that override colloidal interactions and often requires chemical manipulation of the solvent to achieve structural stability^{11,12}. In addition to its fundamental scientific intrigue, the buckling problem has technological relevance in spray drying within various industries. Uncontrolled buckling dampens the release profile of bioactive molecules in drugs¹³

and impedes microencapsulation of additives in food powders¹⁴.

As described by Tsapis et al.¹⁰, particles suspended in an unpinned spherical droplet will pack at the air-water interface to form a viscoelastic shell, which thickens throughout drying. This causes an increase in the pressure drop across the shell eventually leading to its stress-induced sol-gel transition and buckling. Despite the improved understanding of the mechanics of shell formation, little is known about the impact of particle shape on the drying process and corresponding buckling instability. Recent publications have discussed the effect of ionic concentration on the morphology of the dried structure, yet most experiments are limited to the drying of colloidal suspensions containing spherical particles⁹. No significant consideration has been given to the possible role of anisotropy^{15,16} in suppressing buckling, as it was done in the case of coffee-ring formation¹⁷. Changing the morphology of the suspended particles may grant significant control over the mechanical equilibrium of a drying droplet without any modification of solvent chemistry, particle-surface interactions, or even solid fraction^{17,18}.

In this Letter, we investigate the drying of unpinned droplets containing rod-shaped colloidal particles of varying aspect ratio on superhydrophobic surfaces. We observe the suppression of buckling instability in droplets containing rods of high aspect ratio ($AR > 9$), in sharp contrast with the buckling seen for suspensions of low aspect ratio rods ($AR < 9$). All droplet drying begins with isotropic shrinking, during which visible shells are formed which are composed of dense particle packings. We note a striking divergence in the stability of droplets based on the aspect ratio of the suspended rods: shells packed with low aspect ratio rods invariably buckle whereas shells formed by rods of higher aspect ratio retain a spherical shell geometry. This is explained by an increase in permeability attributed to the lower packing efficiency of high aspect ratio rods. On one hand, rods that are shorter and thicker pack into denser shells with low porosity comparable to spherical packings; on the other hand, rigid rods which are thinner and longer jam into highly

^a Cain Department of Chemical Engineering, Louisiana State University, Baton Rouge, Louisiana 70803, USA. E-mail: bbharti@lsu.edu

† Footnotes relating to the title and/or authors should appear here.

Electronic Supplementary Information (ESI) available: additional experimental details, sample calculations and movies of drying droplets. See DOI: 10.1039/x0xx00000x

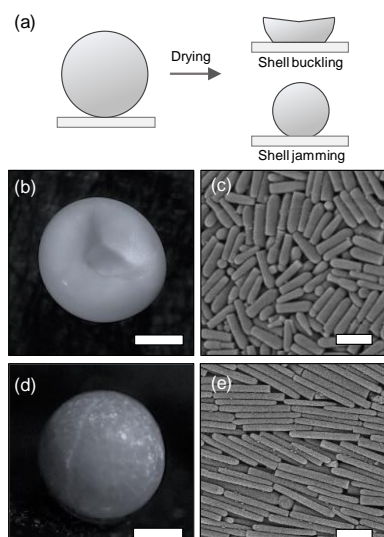


Fig. 1 Evaporation-driven buckling and jamming of droplet shell. (a) During the initial period of isotropic shrinking of the droplet, a shell packed with particles forms which eventually anchors the droplet to the superhydrophobic surface. Shells either (b) buckle if they are composed of (c) low aspect ratio rods ($AR=3.3$) or (d) remain jammed if they are made with (e) high aspect ratio rods ($AR=13.5$). Scale bars are 0.5 mm for (b and d) and 2 μm for (c and e).

permeable shells. Particle morphology is an effective parameter to tune the pressure differential across the droplet shells, preventing the accumulation of internal stresses and offsetting the buckling instability.

In all our experiments, a 3 μL aqueous droplet containing 0.01 volume fraction of rod-shaped silica particles was placed on a superhydrophobic plate and allowed to dry at 20 $^{\circ}\text{C}$ and $42 \pm 4\%$ relative humidity. In these conditions, the radii of all droplets observed was approximately 1/3 of the capillary length of water (2.7 mm), preventing significant distortion of the droplet due to gravity¹⁹. Silica rods were obtained following a known procedure and varying the temperature of synthesis to achieve the required range of aspect ratios²⁰. The surface used is a copper plate rendered superhydrophobic by electrochemical deposition of silver, with a water contact angle of 160 $^{\circ}$ ²¹. The non-wetting properties of the copper substrate were preserved for several weeks. We visualize and record the drying process by high-speed video and image the final structures by stereo microscopy and scanning electron microscopy (SEM). All image analysis and processing was done using the ImageJ software package²². Further experimental details are available in the Electronic Supplementary Information†.

The immediate observation after evaporating 4–6 droplets for each dispersion is the link between aspect ratio of the suspended particles and the morphology of the final dried shell structure, as shown in Fig. 1a. On one hand, droplets containing shorter and thicker rods experience, without fail, a buckling instability which deflates the shell (Fig. 1b–c). On the other hand, droplets dispersed with rods of higher aspect ratio maintain a spherical shell geometry (Fig. 1d–e). The physical basis of shell formation is the packing of particles near the air-water interface occurring at a much faster rate than their diffusion across the droplet volume, leading to a boundary

between the shell and bulk¹⁰. This is the case of a large Péclet number, $Pe = t_{mix}/t_d$, where $t_{mix} = R^2/D$ is the time required for particles with diffusion coefficient D to evenly diffuse across a droplet of radius R , and t_d is the drying time which is ~ 35 –40 minutes in our experiments. A relationship introduced by de la Torre²³ allows to estimate D for rod-shaped particles and determine $t_{mix} > 10^4$ min which confirms that the evaporation-driven assembly of particles at the interface is too rapid for particles to possibly populate the core volume of the droplet. Indeed, the hollow core enveloped by a particulate shell is experimentally observed and imaged by SEM after dissecting the structure (see ESI†).

The dynamics of droplet drying govern the shell formation and its consequent jamming or buckling. The process of assembly of particles near the interface is templated by the droplet shape and their packing is driven by solvent evaporation. While the anisotropic interactions displayed by silica nanorods find analogies with the self-organization of rod-like molecules as in liquid crystals^{24–26}, their bulk arrangement does not reach the ground state. Instead, the end of drying corresponds to an arrested shell configuration which results in either buckling or stable jamming. Approximately 90% of the drying time is characterized by isotropic shrinking, during which a viscoelastic shell forms and thickens near the air-water interface. During the final stage of drying, usually $t > 0.9 t_d$, shells packed with rods of $AR < 9$ buckle as exemplified in Fig. 2a. By contrast, shells formed with rods of $AR > 9$ do not buckle and maintain a quasi-spherical shape, as shown in Fig. 2b. We find that drying colloidal suspensions is overall slower than drying

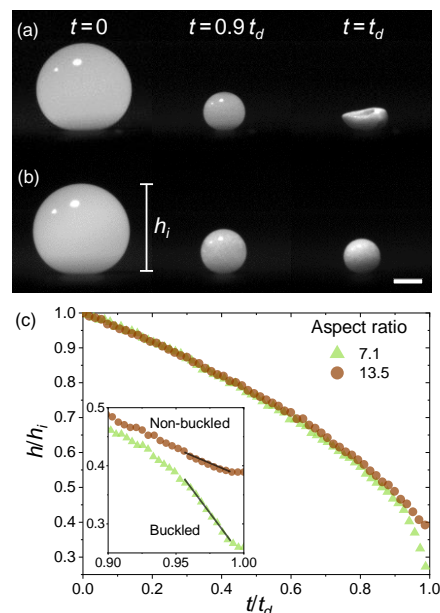


Fig. 2 Snapshots of drying droplets containing rods of aspect ratio (a) 7.1 and (b) 13.5. Scale bar is 0.5 mm. (c) Both droplets shrink linearly, and their drying rates only begin diverging for $t > 0.9 t_d$. The inset shows that buckling of the shell packed with rods of aspect ratio 7.1 (green triangles) greatly increases the drying rate, which remains quasi-steady for the shell made of rods with aspect ratio 13.5 (brown circles) that does not buckle. The slopes of the lines fitted to the experimental data at $t > 0.96 t_d$ are -4.6 and -1.6 respectively for the buckled and stable shells, quantifying the difference in dynamics of evaporation over the final stage of droplet drying.

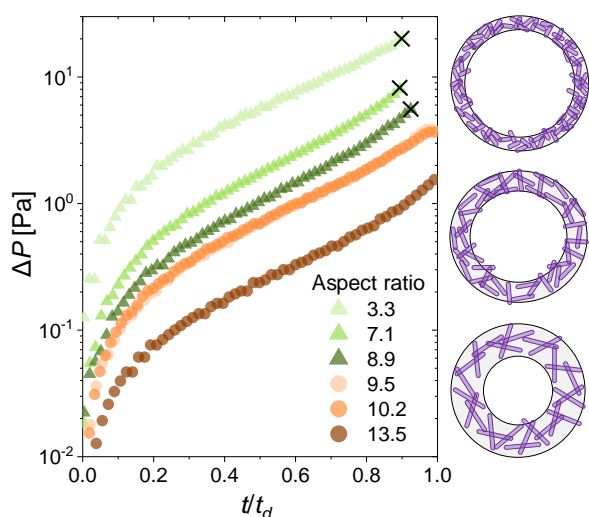


Fig. 3 Change in pressure drop across the shell, calculated throughout drying for droplets containing different aspect ratio rods. The thickening of colloidal shells corresponds to an increase in Darcy's pressure which varies with aspect ratio due to the differences in solvent permeability. The rise in ΔP ends at t_d for stable shells made with high aspect ratio rods (orange-brown circles). The crosses mark the buckling points for the cases of dense shells of lower aspect ratio rods (green triangles), in which ΔP decreases abruptly at $t \sim 0.9 t_d$. The schematics on the right represent the increase in porosity and thickness with increasing aspect ratio of rods.

pure water, which is attributed to a reduction in pristine air-water surface area of the droplet due to the particle packing at the interface (see Fig. S3 in ESI[†]). We quantify overall morphological changes by measuring the height of the droplets h normalized with their initial height h_i and plot the results in Fig. 2c. The initial reduction in h is qualitatively similar for all suspensions as the water evaporates: the droplets shrink and the particles yield and rearrange into thicker shells. The final stage of drying, i.e. at $t > 0.9 t_d$, is of higher relevance in understanding the behaviour of the shell as it undergoes sol-gel transition. The rate of decrease in droplet height varies dramatically as a function of rod aspect ratio as the stability of the formed shells is tested against the completion of the evaporation process. The formed networks of rods experience a sharp dynamical arrest into a jammed out-of-equilibrium structure^{27–29}. Such gelation entails the formation of a porous percolated network with a fraction of solid phase that varies with the aspect ratio of the rods. We find that the density of the packing, as tuned by the shape of the colloids that compose it, may impede percolation. Instead, densely packed rods appear to concentrate stresses on the network because of the low permeability, leading to buckling. Thinner rods ($AR > 9$) form percolated structures which allow interstitial water to squeeze through the shell and evaporate at its outer surface.

The emergence of structural stability as a consequence of increased permeability is non-trivial given that porosity generally decreases the mechanical toughness of materials. The behavior observed here after sol-gel transition does not come from an increase in mechanical strength of the network to sustain buckling loads. Rather, the apparent mechanical equilibrium originates from a significant reduction in the pressure differential across the shell³⁰. Changes in bending

rigidity with anisotropy of particles may also affect the buckling behavior³¹, albeit minimally in the case of unpinned droplets forming 3D shell configurations. To better elucidate the role of aspect ratio, we consider instead the effect of packing density in reducing such pressure drops. A variety of simulations and experimental results have long indicated that the volume fraction of a random close packing is highly dependent on the aspect ratio of the rods^{32–35}. Specifically, increasing the aspect ratio decreases the packing efficiency, with important consequences on the percolation threshold and the pressure difference across the gel. We use the Kozeny-Carman scaling relationship to estimate the liquid permeability k of a porous shell^{36,37}. The scaling of the packing fraction ϕ for spherocylinders as a function of aspect ratio AR is extrapolated from simulations performed by Wouterse et al.³⁸. Values obtained for k range between 10^{-16} – 10^{-14} m² from $AR = 3.3$ to $AR = 13.5$. We use the values for permeability in Darcy's law for flow through porous media to estimate the pressure drop across the shell, $\Delta P = \frac{\eta}{k} \frac{dR}{dt} \delta$. Here, η is the viscosity of the fluid, dR/dt is its volumetric flux and δ is the thickness of the shell. A simple mass balance allows to infer δ as a function of the initial volume fraction of rods in the droplet, the packing fraction in the shell and values of droplet radius measured from image analysis (see ESI[†]). The Darcy's pressure is calculated as δ increases over time until buckling for $AR < 9$ and until the completion of drying for $AR > 9$ (Fig. 3).

The onset of buckling is commonly correlated with a critical δ/R at which ΔP reaches the buckling limit, yet our results point towards a more significant role played by k . Although the thickness of densely packed shells is lower than loose packings (~ 20 μm for $AR = 3.3$; ~ 100 μm for $AR = 13.5$), the estimated ΔP decreases with aspect ratio due to the reduced permeability, as shown in Fig. 4. The values of pressure drop at buckling ΔP_b across the droplet surface are consistent with previous estimations^{10,11} which showed buckling occurring for $\Delta P \sim 100$ Pa. Here, we confirm cases of buckling shells in which the Darcy's pressure drop is between 5 and 20 Pa, for $AR \leq 9$. Shells in structural equilibrium are obtained after a drastic reduction

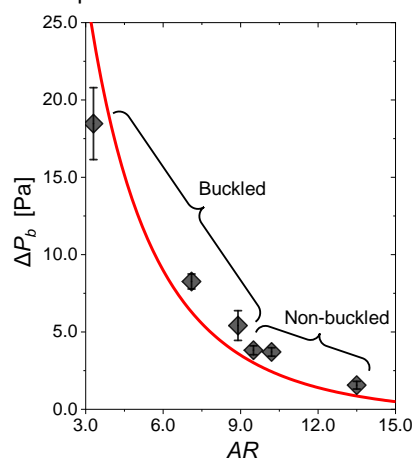


Fig. 4 Pressure drop across the shell at the onset of buckling for $AR = 3.3, 7.1, 8.9$ and at $t = 0.9 t_d$. The error bars are the standard deviation resulting from differences in R measured from image analysis across several experiments. The solid line represents the theoretical pressure drop across a shell packing of rods as a function of aspect ratio.

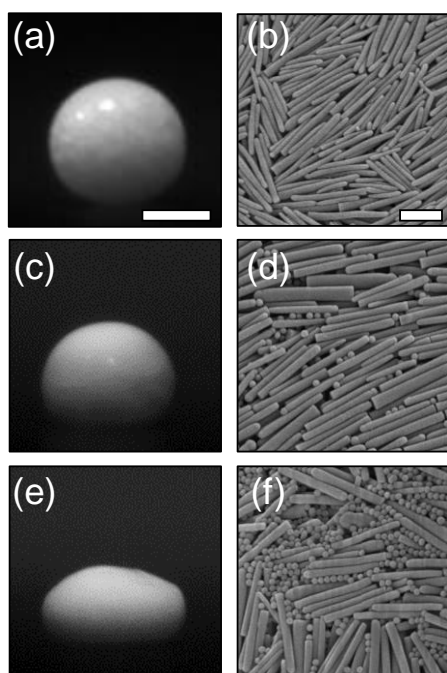


Fig. 5 Buckling induced by pore clogging. Images on the left show dried shells containing (a-b) 0, (c-d) ~ 0.5 and (e-f) ~ 5 sphere-to-rod number ratio; scale bar in (a) represents $300\ \mu\text{m}$. (b), (d) and (f) are SEM showing increased presence of nanoparticles in the shell; scale bar in (b) represents $2\ \mu\text{m}$.

in ΔP to less than $5\ \text{Pa}$, when $AR > 9$. The complex mechanical behaviour of shells is that of a viscoelastic suspension during isotropic shrinking, which is characterized by yielding of particles against capillary forces. The reduced packing density of anisotropic colloids plays a key role in the offset of buckling at the sol-gel transition point. Previous experiments with micron-sized shells show an effect of surface ordering which leads higher aspect ratio rods to buckle³⁹. That is not the case in our system because the size of the rods is much smaller than the equilibrium size of the shell. The dynamically arrested networks show divergent behaviours tuned by porosity: if the packing efficiency is high (low aspect ratio rods), the shell fractures like a soft solid. If the packing is loose (high aspect ratio rods), the particle clusters are fluidized into an isostatic percolated network with low Darcy's pressure.

To further test the poroelastic behaviour of colloidal networks, we introduce Stöber silica nanoparticles to the suspension. The size of the nanoparticles is synthesized to be close to the estimated pore size of a packing of rods with aspect ratio 10.2, which is approximately $170\ \text{nm}$ (see ESI[†]). Note that the total volume fraction of rod particles was kept constant. Increasing the relative number of spherical nanoparticles eventually leads to the buckling of all rod-packed shells, indifferent of the aspect ratio. The 'clogging' of the pores impedes permeation of solvent across the shell and increases ΔP . Such tampered networks experience an accumulation of internal stresses which inevitably ends in the buckling of the shell, as shown in Fig. 5. These experiments corroborate the idea that polydispersity introduces mechanical instability in out-of-equilibrium structures⁴⁰.

Conclusions

The results of our investigation reveal the role of particle morphology in suppressing the buckling of drying droplets of colloidal suspensions. The work indicates particle shape as a tunable parameter for emerging properties of permeability and mechanical equilibrium in dynamically arrested structures. The notion that buckling only occurs at a critical shell thickness is overwritten by the role of porosity: thin but dense packings buckle where thick yet loose ones do not. This may be further extended to other colloidal systems with known or quantifiable packing efficiency, or with particles which are themselves microporous. In addition, we show how shape-anisotropy particles perform specific functions, e.g. pack into mechanically stable shells, at lower volume fractions than spherical particles. From an industrial perspective, this highlights the economic advantage in exploiting the properties conveyed by shape to optimize food and drug micro-processing.

Conflicts of interest

There are no conflicts to declare.

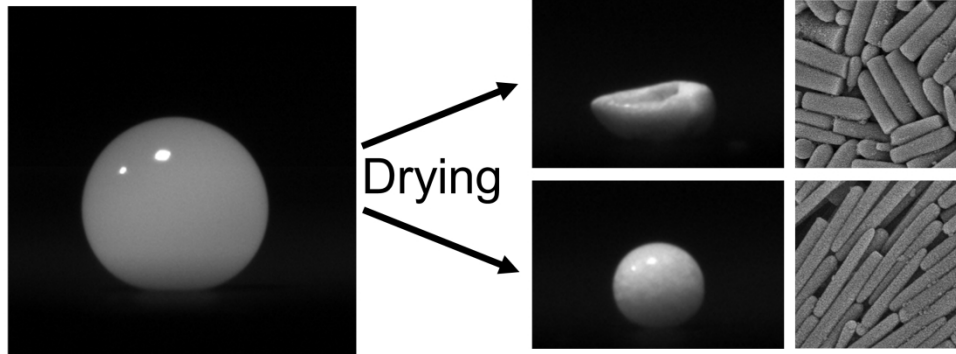
Acknowledgements

We acknowledge the assistance of Andrea Gavilanes and Jin Gyun Lee in performing experiments. BB acknowledges the financial support from NSF-CAREER (CBET-1943986).

Notes and references

- 1 R. D. Deegan, O. Bakajin, T. F. Dupont, G. Huber, S. R. Nagel and T. A. Witten, *Nature*, 1997, **389**, 827–829.
- 2 A. P. Mouat, C. E. Wood, J. E. Pye and J. C. Burton, *Phys. Rev. Lett.*, 2020, **124**, 064502.
- 3 J. G. Lee, V. Porter, W. A. Shelton and B. Bharti, *Langmuir*, 2018, **34**, 15416–15424.
- 4 K. Morinaga, M. Tani and R. Kurita, *Phys. Rev. Res.*, 2020, **2**, 013098.
- 5 Á. G. Marín, H. Gelderblom, D. Lohse and J. H. Snoeijer, *Phys. Rev. Lett.*, 2011, **107**, 085502.
- 6 L. Bansal, A. Miglani and S. Basu, *Phys. Rev. E*, 2016, **93**, 042605.
- 7 R. G. Picknett and R. Bexon, *J. Colloid Interface Sci.*, 1977, **61**, 336–350.
- 8 V. Rastogi, S. Melle, O. G. Calderón, A. A. García, M. Marquez and O. D. Velev, *Adv. Mater.*, 2008, **20**, 4263–4268.
- 9 M. Sperling, O. D. Velev and M. Gradzielski, *Angew. Chemie-International Ed.*, 2014, **53**, 586–590.
- 10 N. Tsapis, E. R. Dufresne, S. S. Sinha, C. S. Riera, J. W. Hutchinson, L. Mahadevan and D. A. Weitz, *Phys. Rev. Lett.*, 2005, **94**, 18302.
- 11 É. Lintingre, G. Ducouret, F. Lequeux, L. Olanier, T. Périé and L. Talini, *Soft Matter*, 2015, **11**, 3660–3665.
- 12 T. Sekido, M. Kappl, H.-J. Butt, S. Yusa, Y. Nakamura and S.

- Fujii, *Soft Matter*, 2017, **13**, 7562–7570.
- 13 A. Ziaee, A. B. Albadarin, L. Padrela, T. Femmer, E. O'Reilly and G. Walker, *Eur. J. Pharm. Sci.*, 2019, **127**, 300–318.
- 14 S. Gouin, *Trends Food Sci. Technol.*, 2004, **15**, 330–347.
- 15 S. C. Glotzer and M. J. Solomon, *Nat. Mater.*, 2007, **6**, 557–562.
- 16 A. Al Harraq, J. G. Lee and B. Bharti, *Sci. Adv.*, 2020, **6**, eaba5337.
- 17 P. J. Yunker, T. Still, M. A. Lohr and A. G. Yodh, *Nature*, 2011, **476**, 308–311.
- 18 M. J. Solomon and P. T. Spicer, *Soft Matter*, 2010, **6**, 1391.
- 19 L. Mahadevan and Y. Pomeau, *Phys. Fluids*, 1999, **11**, 2449–2453.
- 20 A. Kuijk, A. van Blaaderen and A. Imhof, *J. Am. Chem. Soc.*, 2011, **133**, 2346–2349.
- 21 C. Gu, H. Ren, J. Tu and T.-Y. Zhang, *Langmuir*, 2009, **25**, 12299–12307.
- 22 C. A. Schneider, W. S. Rasband and K. W. Eliceiri, *Nat. Methods*, 2012, **9**, 671–675.
- 23 M. M. Tirado, C. L. Martínez and J. G. de la Torre, *J. Chem. Phys.*, 1984, **81**, 2047–2052.
- 24 V. G. Nazarenko, O. P. Boiko, H.-S. Park, O. M. Brodyn, M. M. Omelchenko, L. Tortora, Y. A. Nastishin and O. D. Lavrentovich, *Phys. Rev. Lett.*, 2010, **105**, 17801.
- 25 I. I. Smalyukh, Y. Lansac, N. A. Clark and R. P. Trivedi, *Nat. Mater.*, 2010, **9**, 139–145.
- 26 Y.-K. Kim, X. Wang, P. Mondkar, E. Bukusoglu and N. L. Abbott, *Nature*, 2018, **557**, 539–544.
- 27 R. C. Kramb, R. Zhang, K. S. Schweizer and C. F. Zukoski, *Phys. Rev. Lett.*, 2010, **105**, 055702.
- 28 C. K. Mishra, A. Rangarajan and R. Ganapathy, *Phys. Rev. Lett.*, 2013, **110**, 188301.
- 29 A. P. R. Eberle, N. J. Wagner and R. Castañeda-Priego, *Phys. Rev. Lett.*, 2011, **106**, 105704.
- 30 H. Tsurusawa, M. Leocmach, J. Russo and H. Tanaka, *Sci. Adv.*, 2019, **5**, eaav6090.
- 31 P. J. Yunker, M. Gratale, M. A. Lohr, T. Still, T. C. Lubensky and A. G. Yodh, *Phys. Rev. Lett.*, 2012, **108**, 228303.
- 32 A. Ekman, A. Miettinen, T. Tallinen and J. Timonen, *Phys. Rev. Lett.*, 2014, **113**, 268001.
- 33 A. Donev, I. Cisse, D. Sachs, E. A. Variano, F. H. Stillinger, R. Connelly, S. Torquato and P. M. Chaikin, *Science*, 2004, **303**, 990 LP – 993.
- 34 A. Donev, R. Connelly, F. H. Stillinger and S. Torquato, *Phys. Rev. E*, 2007, **75**, 051304.
- 35 J. O. Freeman, S. Peterson, C. Cao, Y. Wang, S. V Franklin and E. R. Weeks, *Granul. Matter*, 2019, **21**, 84.
- 36 P. C. Carman, *Trans. Inst. Chem. Eng.*, 1937, **15**, 150–166.
- 37 D. M. E. Thies-Weesie and A. P. Philipse, *J. Colloid Interface Sci.*, 1994, **162**, 470–480.
- 38 A. Wouterse, S. R. Williams and A. P. Philipse, *J. Phys. Condens. Matter*, 2007, **19**, 406215.
- 39 R. Mondal, A. Das, D. Sen, D. K. Satapathy and M. G. Basavaraj, *J. Colloid Interface Sci.*, 2019, **551**, 242–250.
- 40 D. Sen, J. Bahadur, S. Mazumder and S. Bhattacharya, *Soft Matter*, 2012, **8**, 10036.



787x406mm (96 x 96 DPI)